Effect of tempering temperature on very high cycle fatigue properties of high strength steel

H. Oguma[1], T. Nakamura[1]
[1]*Div. of Mech. & Space Eng. Hokkaido University, Sapporo, Japan;*
E-mail: Hiroyuki.Oguma@eng.hokudai.ac.jp

Abstract

To investigate the effect of tempering temperature on the very high cycle fatigue properties, uniaxial tension-compression fatigue tests of Ni-Cr-Mo steel (SNCM439, corresponding to AISI 4340 steel) which had been tempered, either at 433K (640Hv) or 573K (543Hv) were carried out. The fracture origins in 10^4 - 10^5 cycle range located at the specimen surface, whereas in the 10^5 - 10^8 cycle range the fracture origins were sub-surface. The fatigue limits for the surface-initiated failures were in good agreement with the conventional expression $\sigma_{w0} \approx 1.6 \cdot Hv$. However, in the the fatigue limit in the sub-surface crack-initiation range was lower for the harder condition. SEM examination showed that the type of inclusion at the failure origin depended upon the tempering temperature. This dependency may be the cause of the unusual relation between hardness and fatigue strength in the very high cycle fatigue range.

1. Introduction

In recent years the very high cycle fatigue (VHCF) [1, 2] of high strength steel has become a topic of great interest for many advanced structural designs. In the lower fatigue life region, the origin of fatigue fracture is usually at the surface, whereas for longer fatigue lifetimes fatigue origins are generally sub-surface in nature. It has been reported that the sub-surface fractures occur at a lower stress level than the surface-initiated fracture. As yet there is not a clear understanding of the mechanism that is responsible for the fatigue process in VHCF. Basically, fatigue strength in high cycle regime become higher with increases of tensile strength and hardness. However, more careful examinations are needed whether the relation can be applied for the VHCF. The present paper presents the results of an investigation into the effect of tempering temperature on very high cycle fatigue properties of high strength steel.

2. Experimental procedure

The material used in this study was Ni-Cr-Mo steel (SNCM439 corresponding to AISI 4340 steel). The chemical composition is given in Table 1. The material was obtained as a circular rod of diameter of 17 mm. The heat treatment of the as-received rod was as follows: normalizing at 1133K for 3.6ks (air-cooled), followed by quenching at 1123K for 3.6ks (oil-cooled) and then tempering. The tempering conditions were as follows; (1) 433K for 7.2ks and then air-cooled (designate LT for Low-Tempering temperature) or (2) 573K for 7.2ks and then

water-cooled (designated HT for High-Tempering temperature). Fig. 1 shows the microstructures of these materials after the heat treatment taken with a scanning electron microscope (SEM). The microstructures of both materials were tempered martensite. In LT material, the size of prior austenite grains and widths of martensite block were 10 to 15 μm and 1 to 2 μm, respectively. On the other hand, in HT material, carbide separated out in martensite, and microstructure looks finer. The mechanical properties for both conditions are given in Table 2.

Table 1: Chemical composition.

[mass %]

C	Si	Cu	Mn	P	S	Ni	Cr	Mo
0.40	0.22	0.18	0.78	0.020	0.013	1.78	0.83	0.20

Table 2: Mechanical properties.

Material	Tempering Temperature [K]	Tensile Strength [MPa]	0.2% Proof Stress [MPa]	Vickers Hardness [HV]
LT	433	2274	1515	640
HT	573	1737	1283	543

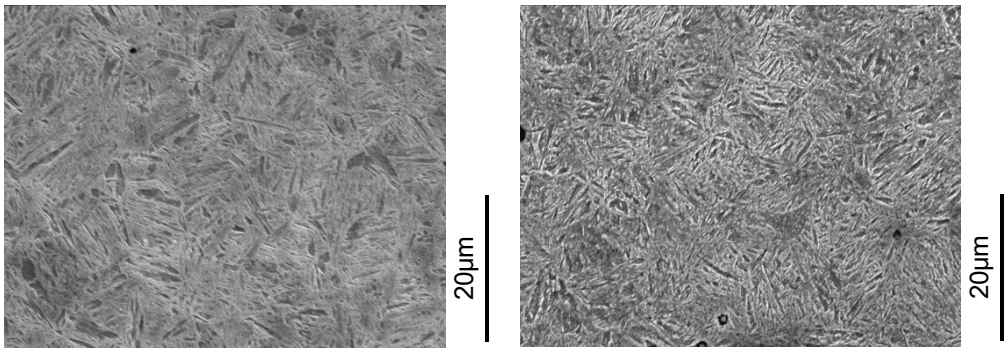

(a) Material LT (433K) (b) Material HT (573K)

Figure 1: Microstructures observed by SEM.

Fig. 2 shows the shape and dimensions of the fatigue specimen. After lathe turning the material into an hourglass-type test piece of 4.1 mm minimum diameter, each specimen was polished with #120 to #1500 emery paper. Uniaxial tension-compression fatigue tests were carried out in air under sinusoidal waveform loading at a stress ratio of –1 at room temperature using a electro-servo-hydraulic-testing machine at 40Hz (for high stress), or 80 - 120 Hz (for low stress). The tests were terminated at 10^8 cycles.

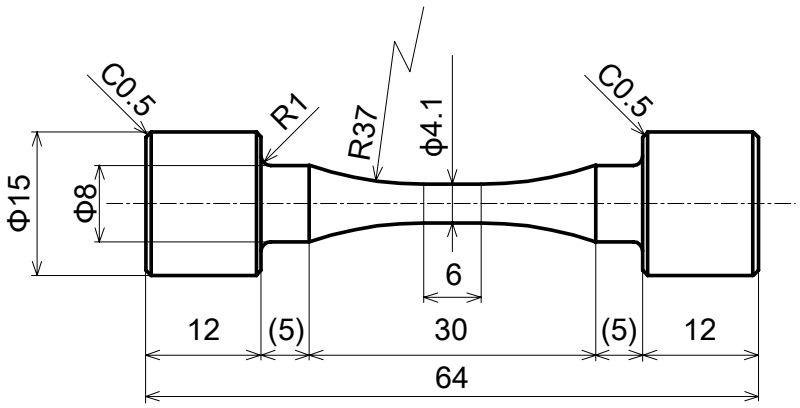

Figure 2: Specimen configuration.

3. Experimental results

The number of cycles to failure N_f as a function of stress amplitude σ_a is shown in Fig.3 for both tempering conditions. Data of LT material is indicated by the square and that of HT material by the circle. A filled symbol indicates a surface-initiated fracture, and an open symbol indicates a sub-surface initiated fracture. For both materials, surface-initiated fracture dominates in short life regime. The lives of sub-surface fractures range from 10^5 to 10^8 cycles. It is seen that sub-surface fatigue can take place at a relatively low number of cycles in this material.

The fatigue strength of surface-initiated fracture was defined as the average of the minimum stress in the surface-initiated fractures and the maximum stress of the sub-surface fractures (but the data is from below the stress where surface-initiated fractures occurred). As a result, following values were obtained: 1025 MPa for LT, 925 MPa for HT. These values are proportional to the Vickers hardness, and the relation was in good agreement with the conventional expression of $\sigma_{w0} \approx 1.6 \cdot Hv$ where σ_{w0} is the fatigue limit of the smooth specimen without stress concentration (in MPa) and HV is the Vickers hardness (in kgf/mm^2).

The S-N curves for the sub-surface fracture were downward-sloping, and did not exhibit an apparent fatigue limit even at 10^8 cycles. Consequently, the strength at 10^8 cycles was defined as the average of the stress data at 10^8 cycles and the minimum stress among the fracture data below 10^8 cycles. The resultant values are 675 MPa for LT and 775 MPa for HT. Namely, the strength at 10^8 of HT is higher than that of LT, and in contrast to the generally observed behavior, the harder material exhibited the lower fatigue strength of sub-surface fracture. However in view of the small number of tests involved, any conclusions should be drawn with caution, for as will be shown the origin is strongly dependent upon the nature and size of the initiating inclusion.

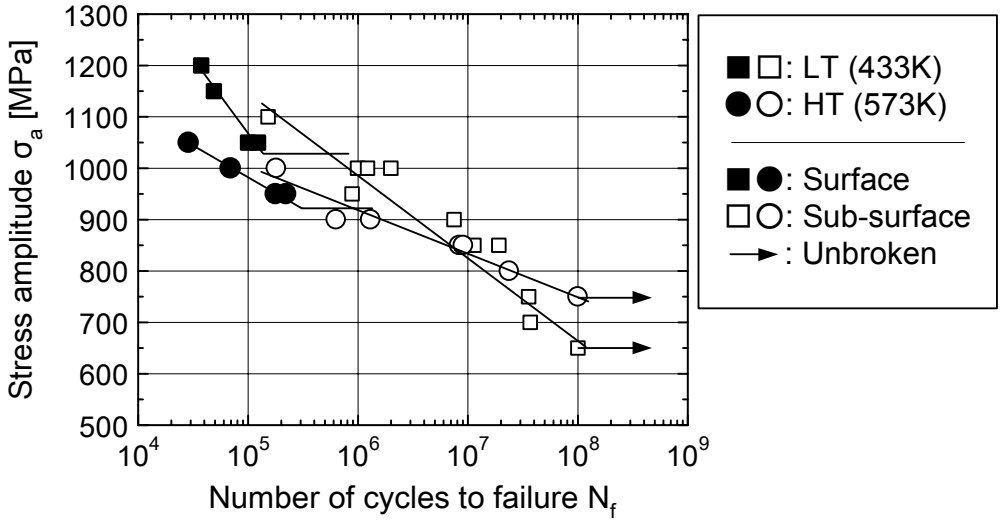

Figure 3: S-N diagram.

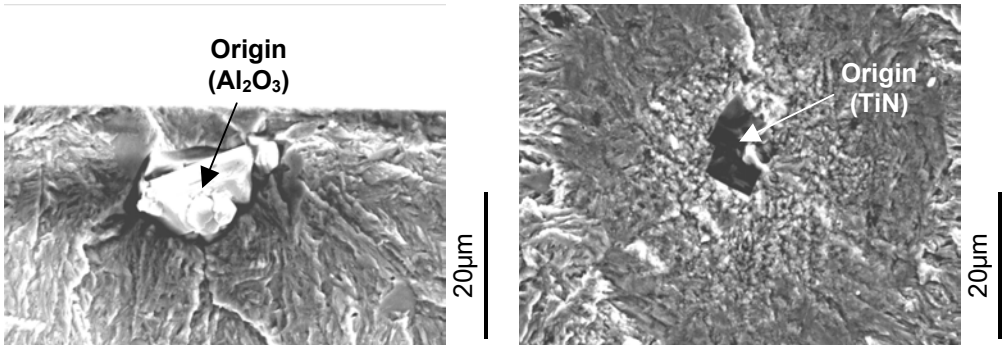

(a) Surface-initiated fracture (LT, σ_a = 1200 MPa, N_f = 3.74*10^4)

(b) Sub-surface fracture (LT, σ_a = 850 MPa, N_f = 1.91*10^7)

Figure 4: Fracture origins for LT material (433K).

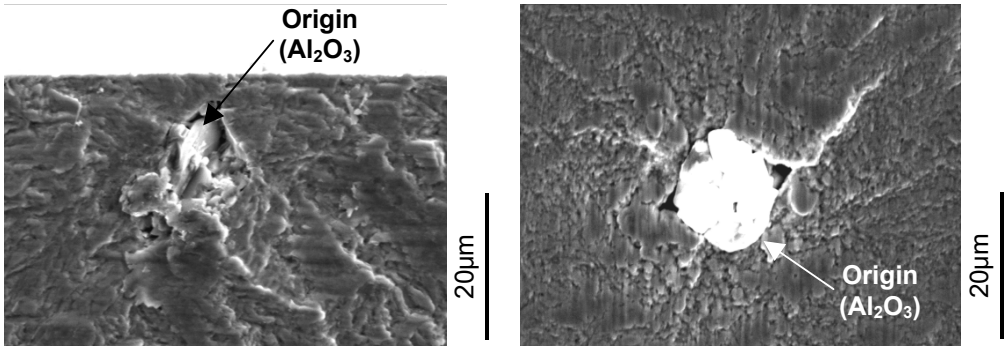

(a) Surface-initiated fracture (HT, σ_a = 950 MPa, N_f = 2.21*10^5)

(b) Sub-surface fracture (HT, σ_a = 800 MPa, N_f = 2.37*10^7)

Figure 5: Fracture origins for HT material (573K).

Fracture surfaces were observed by using SEM. Fig. 4 and Fig. 5 are magnified photographs of crack initiation sites. Almost all the fracture origins were located at inclusions of TiN or Al_2O_3. The following classification system, Table 3, was used to distinguish between the various sizes of the inclusions.

Table 3: Classification of inclusion sizes.

Class	Size
CLASS 1	0-10μm
CLASS 2	10-20μm
CLASS 3	20-30μm
CLASS 4	30-40μm

4. Discussion

In order to consider the effect of the fracture origin size on fatigue crack propagation lives, the relation between the initial stress intensity factor range ΔK_{ini} and the fatigue life N_f divided by the fracture origin size are investigated [3]. The ΔK_{ini} was calculated from the following equations [4]:

$$\Delta K_{ini} = 0.65\Delta\sigma\sqrt{\pi\sqrt{area}} \quad \text{: Surface-initiated fracture} \qquad (1)$$

$$\Delta K_{ini} = 0.50\Delta\sigma\sqrt{\pi\sqrt{area}} \quad \text{: Sub-surface fracture} \qquad (2)$$

where $\Delta\sigma = \sigma_{\max}$.

In the equations, the *area* is the projected area of the fatigue crack origin (in this study, the inclusion) on the principal stress plane. The data are shown in double logarithmic chart, Fig. 6. The distribution range of the data in Fig.6 is smaller than that in the S-N diagram (see Fig. 3). For both tempering conditions, the data for the surface-initiated fractures in Fig. 6 are similar, however, a greater dissimilarity is found in the case of the sub-surface fracture. Although there is appreciable scatter, the data for the LT material is distributed at a lower ΔK_{ini} region than in the case of the HT material (in figures - open symbols). The data points for each material were fitted with a straight line of the form shown in Eq. (3) which was obtained by the use of the least-square method.

$$\log(\Delta K_{ini}) = -\frac{1}{m}\log\left(\frac{N_f}{a_0}\right) + \frac{1}{m}\log\left\{\frac{2}{C(m-2)}\right\} \qquad (3)$$

where a_0: crack origin size i.e., $\sqrt{area}$ of the inclusion.

Because in Fig. 6 the slope for LT material is larger than that of HT material, the difference in ΔK_{ini} values increases in long life regime.

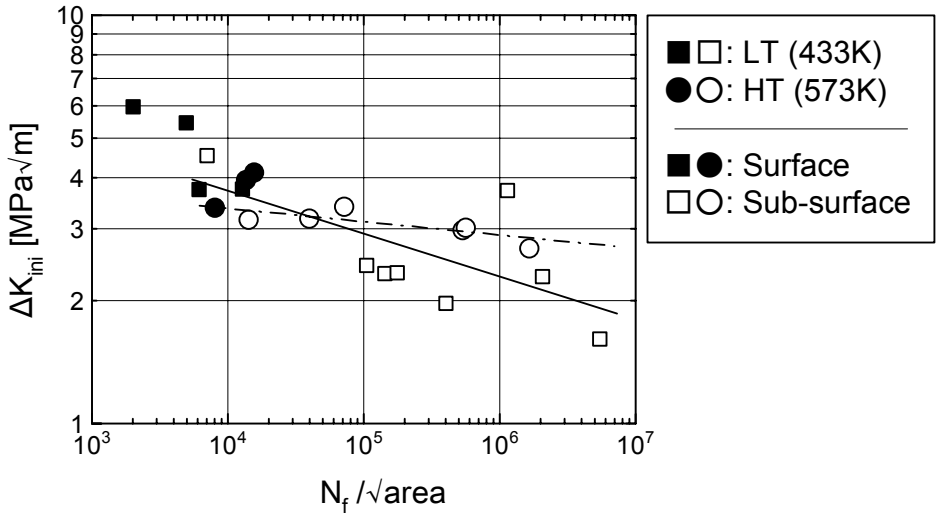

Figure 6: Relation between ΔK_{ini} and $N_f/\sqrt{area}$.

Fig.7 shows ΔK_{ini} –$N_f/\sqrt{area}$ diagram classified by the type and the size of inclusions. The type of crack-initiating inclusions is indicated by superscript of "T" for TiN and "A" for Al_2O_3 in the diagram. It can be seen that in the higher ΔK_{ini} region the crack origins were located at Al_2O_3 inclusions, whereas in the lower ΔK_{ini} region the fracture origins were located at TiN inclusions.

With respect to the size of inclusion at failure origin, in the HT material only Al_2O_3 inclusions of CLASS 2 size acted as failure origins. However, for the LT material, all sizes of inclusions except for CLASS 2 were crack origins, and both types of inclusions were found. Namely, the smaller TiN inclusions can be fracture origins in the harder material. Additionally in the material LT, smaller inclusions show lower ΔK_{ini}. Therefore, a crack propagation threshold probably has a size dependency in the sub-surface fracture. Since all of the tested specimens were machined from the same ingot, no bias as to the type and size of the inclusions can be assumed. It appears therefore that in the case of a sub-surface failure, the tempering temperature can affect the type of inclusion that acts as a fatigue crack origin.

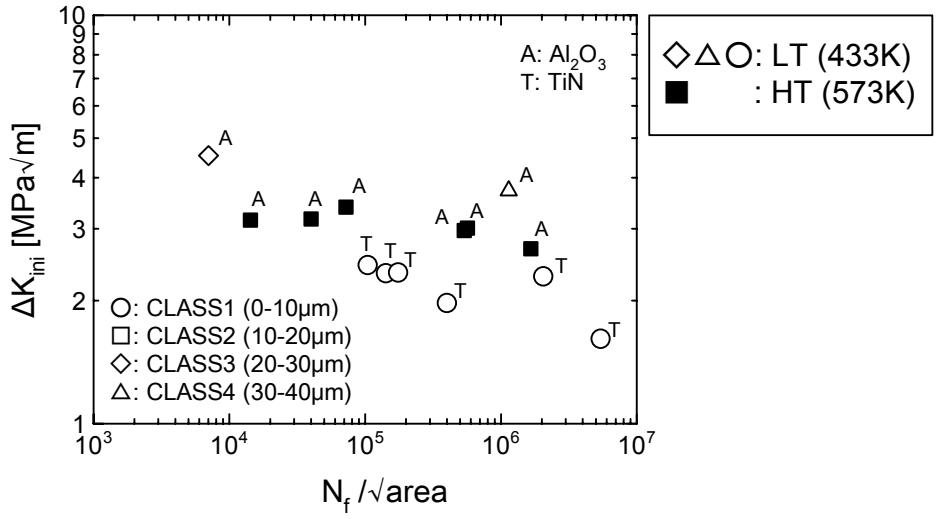

Figure 7: ΔK_{ini} - $N_f/\sqrt{area}$ diagram for the sub-surface fracture classified by the type and the size of inclusions.

5. Conclusions

Uniaxial tension-compression fatigue tests of high strength steel tempered at different tempering temperatures (433K and 573K) were conducted into the very high cycle regime, and following results were obtained:

(1) The fatigue strength of surface-initiated fracture for both tempering conditions was proportional to the Vickers hardness, and was in good agreement with the conventional expression of $\sigma_{w0} \approx 1.6 \cdot Hv$.

(2) In the very high cycle regime, the material tempered at the lower temperature showed lower fatigue strength, that is, the harder material exhibited the lower fatigue strength.

(3) In the case of a sub-surface fracture, the tempering temperature can affect the type of inclusion that acts as a fatigue crack origin. This can be the reason of the unusual relation as mentioned in (2) between the fatigue strength and the hardness in the very high cycle regime.

Acknowledgments
The authors wish to acknowledge the support of a Grant-in Aid for Scientific Research (B(2), 2006-2008) from the Ministry of Education, Culture, Sports, Science and Technology, Japan.

Special thanks are due to Professor A. J. McEvily (University of Connecticut) for constructive comments and suggestions, to S. Ikeda and K. Nakamura (Hokkaido University) for help with the fatigue tests and the SEM observations.

References

[1] Y. Murakami, T. Nomoto, T. Ueda, On the mechanism of fatigue failure in the superlong life regime ($N > 10^7$ cycles). Part I: Influence of hydrogen trapped by inclusions, Fatigue Fract Engng Mater Struct, Vol. 23, pp.893-902, 2000

[2] S. Nishijima, K. Kanazawa, Stepwise S-N curve and fish-eye failure in gigacycle fatigue, Fatigue Fract Engng Mater Struct, Vol. 22, pp.607-607, 1999

[3] S. Omata, Evaluation of fatigue properties in the ultra-high-cycle regime of steels for crankshafts based on crack propagation characteristics, Proceedings of the Third International Conference on Very High Cycle Fatigue (VHCF-3), pp.306-313, 2004

[4] Y. Murakami, Analysis of Stress Intensity Factors of Modes I, II and III for Inclined Surface Cracks of Arbitrary Shape, Eng. Fract. Mech., Vol. 22, pp.101-114, 1985